SUPPORTING ONLINE MATERIAL

MATERIALS AND METHODS

Viral vectors preparation

A replication-deficient retroviral vector based on the Moloney murine leukemia virus was used to express RFP under a CAG promoter (*1*). Retroviral particles were assembled using three separate plasmids containing the capside (CMV-vsvg), viral proteins (CMV-gag/pol) and the transgene (CAG-RFP). For channelrhodopsin-2 expression, retroviral particles were prepared by using a Ubi-ChR2-GFP plasmid (kindly provided by S. Ge, SUNY Stony Brook)**.** Plasmids were transfected onto HEK 293T cells using deacylated polyethylenimine. Virus-containing supernatant was harvested 48 h after transfection and concentrated by two rounds of ultracentrifugation. Virus titer was typically ~10^5 particles/µl.

Animals and surgery for retroviral delivery

Female C57Bl/6J mice 6–7 weeks of age were housed at 4 mice per cage, with two running wheels. Running wheel housing started 2-4 days before surgery and continued until the day of slice preparation. For surgery, mice were anesthetized (150 µg ketamine/15 µg xylazine in 10 µl saline/g), and virus (1 µl at 0.15 µl/min) was infused into the dorsal area of the right dentate gyrus using sterile microcapillary calibrated pipettes and stereotaxic references (coordinates from bregma: -2 mm anteroposterior, -1.5 mm lateral, -1.9 mm ventral). Animals were killed for acute slice preparation at the indicated times. Experimental protocols were approved by the Institutional Animal Care and Use Committee of the Fundación Instituto Leloir according to the Principles for Biomedical Research involving animals of the Council for International Organizations for Medical Sciences and provisions stated in the Guide for the Care and Use of Laboratory Animals.

Slice preparation

Mice were anesthetized and decapitated at 4 or 8 weeks post injection (wpi) as indicated. Brains were removed into a chilled solution containing (mM): 110 choline-Cl^-, 2.5 KCl, 2.0 NaH_2PO_4, 25 $NaHCO_3$, 0.5 $CaCl_2$, 7 $MgCl_2$, 20 dextrose, 1.3 Na^+-ascorbate, 0.6 Na^+-pyruvate, and 4 kynurenic acid. The right hippocampus was dissected and coronal slices (400 µm thick) were cut in a vibratome and transferred to a chamber containing artificial cerebrospinal fluid (ACSF; mM): 125 NaCl, 2.5 KCl, 2 NaH_2PO_4, 25 $NaHCO_3$, 2 $CaCl_2$, 1.3 $MgCl_2$, 1.3 Na^+-ascorbate, 3.1 Na^+-pyruvate, and 10 dextrose (315 mOsm). Slices were bubbled with 95% O_2/5% CO_2 and maintained at 30°C for >1 hour before experiments started.

Time-lapse calcium imaging

Bulk loading of the dye. Under differential interference contrast (DIC) visual guidance, a pipette containing 400 µM Oregon green BAPTA-1 AM (OGB-1 AM, dissolved in 98% DMSO and 2% pluronic F-127 acid) was positioned on the surface of the slice at the GCL. The dye was applied with 1 s pulses of positive pressure every 30-50 µm along the GCL within the field of view (**Fig. S1A).** Recordings started >30 minutes after loading.

Imaging. Fluorescence excitation and emission were bandpass filtered by dual 470-495/510-550 nm (OGB-1) and 535-555/570-625 nm filters (RFP). Emission fluorescence was collected with a digital camera mounted on an Olympus BX61WI microscope with a 40x (N.A. 0.8) water immersion objective. Calcium image acquisition (20 ms exposure at 10 Hz) was performed using the Xcellence pro software. Fluorescence changes after stimulation of the medial perforant path (mPP) were calculated non-ratiometrically as $\Delta F/F_0$, where F_0 is the resting fluorescence and ΔF is the time-dependent change in fluorescence. Because of the short duration of each individual trial, no correction for bleaching was made. Calcium transients were monitored over the entire field of view and frames corresponding to the peak $\Delta F/F_0$ were selected. Peak $\Delta F/F_0$ was averaged across

five trials (**Fig. S1B**) for each stimulus intensity. An RFP fluorescence image was taken between calcium imaging trials in order to overlay immature neurons with the corresponding $\Delta F/F_0$ for each trial. MPP stimulation was performed placing a steel monopolar electrode in the middle of the molecular layer, applying current pulses ranging from 5 to 150 µA (100 µs). At the end of each experiment 4 mM kynurenic acid was applied to the bath in order to rule out any possible direct electrical stimulation of the recorded neurons.

Image processing. Images were analyzed with the NIH ImageJ (http://rsb.info.nih.gov/ij/) software. Recruited GCs were extracted as ensemble maps from average peak $\Delta F/F_0$ images and RFP fluorescence images in a three-step process (**Fig. S1B,C**). First, the image was correlated with a circular template (5.6 µm in diameter). Second, the resulting image was transformed into a binary image by imposing a threshold (~0.13; adjusted for each experiment). Last, each recruited cell was defined as a cluster of a minimum number of adjacent pixels (~50 pixels for images captured with the 40x objective, adjusted for each experiment). A similar analysis has been previously reported (*2*). Active 4 wpi GCs were identified by overlay of RFP fluorescence and calcium imaging resulting ensemble maps. Note that for the imaging experiments, RFP^- neurons were considered as mature GCs, which strictly represents a population of neurons highly enriched in mature GCs with a minor contribution of unlabeled immature neurons that may produce a slight overestimate in the activation profile of this population.

Somatic calcium transients report the spiking of GCs in response to mPP stimulation. Simultaneous loose patch recordings and calcium imaging of GCs showed that somatic calcium transients correlate with the occurrence of individual action potentials (**Fig. S1D**). For calcium profiles, averaged transients of fluorescence from regions of interest were corrected for background fluorescence by subtracting the fluorescence of an adjacent area of same dimensions. In addition, spiking evoked by mPP stimulation elicits calcium transients with similar amplitude and kinetics in 4 wpi and mature GCs (**Fig. S1E,F**).

Electrophysiological recordings

Recorded neurons were visually identified by fluorescence and infrared DIC videomicroscopy. The mature neuronal population encompassed RFP^- neurons localized in the outer third of the GCL (*3*). Whole-cell recordings were performed using microelectrodes (4-5 MΩ) filled with (mM): 130 CsOH, 130 D-gluconic acid, 3 $MgCl_2$, 0.2 EGTA, 1 NaCl, 10 HEPES, 4 ATP-tris, 0.3 GTP-tris, 10 phosphocreatine. Final Cl^- concentration was adjusted, according to neuronal age, using CsCl to match the values calculated after measurements of reversal potential (**Fig. S3,** see below), to 10.1 mM (young neurons) and 7.4 mM (mature neurons). Loose-patch recordings were performed with ACSF-filled patch pipettes (8–10 MΩ). Field recordings were performed using patch pipettes (2–4 MΩ) filled with 3M NaCl. All recordings were obtained using Axopatch 200B amplifiers, digitized, and acquired at 20 KHz onto a personal computer using the pClamp 9 software. Membrane capacitance and input resistance were obtained from current traces evoked by a hyperpolarizing step of 10 mV. Series resistance was typically 10 – 20 MΩ, and experiments were discarded if higher than 30 MΩ.

Reversal potential of GABAergic responses was measured by gramicidin-perforated patch recordings and local GABA (20 μM) picospritzer application (**Fig. S3**). Measured values were used to calculate the physiological range of intracellular Cl^- concentration of young and mature GC. Stock solutions of gramicidin were prepared at 5 mg/ml in ethanol. The pipet solution contained (mM): 150 KCl, 5 HEPES and 5 HEPES-Na^+ (pH 7.4, 300 mOsm). Gramicidin was added fresh to a final concentration of 10 μg/ml and backfilled into the recording pipets (4 MΩ). Recordings displaying series resistance <100 MΩ were used for analysis. The voltage-clamp potential was corrected off-line by calculating the voltage drop across the series resistance.

Calibration of input strength for GC activation

The input strength is proportional to the number of activated mPP axons. The slope of the field excitatory postsynaptic potential (fEPSP) increases linearly with the number of activated axons (*4*). Therefore, for experiments involving GC activation (**Figures 1,2,3 and S8**), input strength was assessed as percentage fEPSP slope (**Fig. S2A-C**). For this purpose, one field-recording microelectrode was placed in the molecular layer to record the fEPSP and another one was placed in the granule cell layer to record the population spike (pop spike) in response to mPP stimulation. To compare input strengths across experiments, the fEPSP slope elicited at any given stimulus intensity was normalized to the fEPSP slope evoked at a stimulus intensity that evokes a maximal pop spike (100 %). The input strength was always assessed and calibrated in the absence of blockers. Thus, for a given input strength within a slice, the number of mPP axons stimulated in control conditions or in the presence of PTX were the same. In calcium imaging experiments (**Fig. 1**) the fEPSP was recorded in the granule cell layer. A similar approach for input strength calibration has been previously used (*4*).

Activation curves

To construct GC activation curves in electrophysiology experiments, loose patch recordings were performed as the mPP was stimulated at increasing intensities (**Fig. 2**). Five to 10 trials were performed to measure spiking probability at each stimulus intensity (**Fig. 2B**). The threshold input strength (50% spiking probability) for individual neurons was interpolated by fitting their spiking probability plotted against input strength to the sigmoid function: $y = 100 \div \left(1 + 10^{(x_o - x)p}\right)$, where x_0 is the threshold input strength and p the slope at x_0 (**Fig. 2C**). The activation curve of a neuronal population (**Fig. 2D**) is the cumulative distribution of input strengths that elicit 50% spiking probability for each neuron.

Percentage of activation in calcium imaging experiments was calculated as the number of activated cells of a certain population (RFP^+ or RFP^-) at a particular input strength (% $fEPSP_{slope}$) over the maximum number of activated GCs of that population in the slice in the presence of PTX (**Fig. S2D,E**).

Evoked postsynaptic currents and conductances

After measuring activation in the loose patch configuration, the same neurons were subsequently recorded in the whole cell configuration (**Fig. 3**). Evoked monosynaptic EPSCs and disynaptic IPSCs were recorded after mPP stimulation at the threshold input strength. To minimize the contribution of IPSCs mediated by direct stimulation of inhibitory axons we only considered experiments in which KYN (6 mM, bath applied at the end of the experiment) blocked >70% of IPSCs **(Fig. S4 and S8).** EPSCs were isolated by voltage clamping GCs at the reversal potential of the IPSC measured for each individual neuron (-55.7 ± 1.3 mV, n = 7 for 4 wpi and -61.9 ± 2.5, n = 8 for mature GCs). In turn, disynaptic IPSCs were recorded at the reversal potential of the EPSC (-4.7 ± 3.5 mV, n = 7 for 4 wpi and -5.0 ± 3.5, n = 8 for mature). When present, direct monosynaptic IPSC recorded in KYN (always <30% of the peak IPSC amplitude) was subtracted from the IPSC. Peak synaptic excitatory and inhibitory conductances were computed as the peak of the EPSC or IPSC divided by the driving force at which the synaptic currents were recorded. For each cell, the spike timing used to calculate the contribution of excitation and inhibition required for the neuron to fire an action potential was an average of the time of spike occurrence elicited at threshold in loose patch recordings.

To separately study IPSCs arising at the dendritic and perisomatic domains (**Fig. S5**) we took advantage of the Cl^- gradient imposed by the patch pipette. We used a symmetrical chloride internal solution containing (mM): 140 CsCl, 2 $MgCl_2$, 0.1 EGTA, 5 NaCl, 10 HEPES, 4 ATP-tris, 0.3

GTP-tris, 10 phosphocreatine. Under conditions of symmetrical Cl^-, the predicted reversal potential for perisomatic IPSCs is 0 mV while that of dendritic IPSCs would be shifted to more hyperpolarized values (*1*). Stimulating electrodes were placed in the granule cell layer and in the molecular layer to activate perisomatic or dendritic inhibition in the presence of 6 mM kynurenic acid to block glutamatergic transmission. IPSCs were recorded in whole-cell configuration at -70 mV and at 0 mV. As expected, stimulation of both perisomatic and dendritic inhibition evoked fast and slow inward IPSCs at -70 mV respectively. At 0 mV only dendritic inhibition evoked slow outward IPSCs, while perisomatic inhibition was at the reversal potential.

Optogenetics

Hippocampal slices containing adult-born GCs expressing channelrhodopsin-2 (ChR2) were prepared four weeks after retroviral delivery. ChR2 was stimulated using the epifluorescence pathway of the upright microscope (100 W Hg lamp, FITC filter, 63X objective) controlled by an electronic shutter commanded through the acquisition software. Whole-cell recordings were carried out in CA3 pyramidal cells in slices containing several GCs that displayed GFP (ChR2) expression as previously described (*5*). Light pulses (10 ms) were delivered at 1 Hz while postsynaptic currents were recorded in voltage-clamp. For recordings obtained from pyramidal cells, the internal pipette solution was the one described for EPSC measurements on mature GCs (**Fig. S7**).

Input integration measurements

To quantify input integration (**Fig. 4H-J**), the probability that a GC was recruited by both inputs was computed as the number of GCs belonging to the RFP^+ or RFP^- population within the field of view recruited by both inputs 1 and 2 at each particular input strength, normalized to the total number of GCs of that population recruited at that strength by either input. To pool data from different

slices, input strength was normalized for each particular stimulus intensity as the percentage of active cells divided by the total number of responding cells in the slice (**Fig. S2D-E**). The total number of responding GCs was obtained at the end of the experiment after applying PTX (100 µM) and delivering a strong stimulus to the mPP (100-150 µA).

To validate that inputs 1 and 2 were independent, we compared for each slice the sum of the fEPSP slopes obtained for each individual input to the fEPSP slope obtained with both inputs activated simultaneously (**Fig. S6**). Stronger stimulus intensities displayed decreased independence and were, therefore, avoided.

Statistical analysis

Significant differences were assessed by two-tailed *t*-test, Kolmogorov-Smirnov test, one-way or two-way ANOVA and Bonferroni's post hoc test, as indicated in the figure legends.

Fig. S1

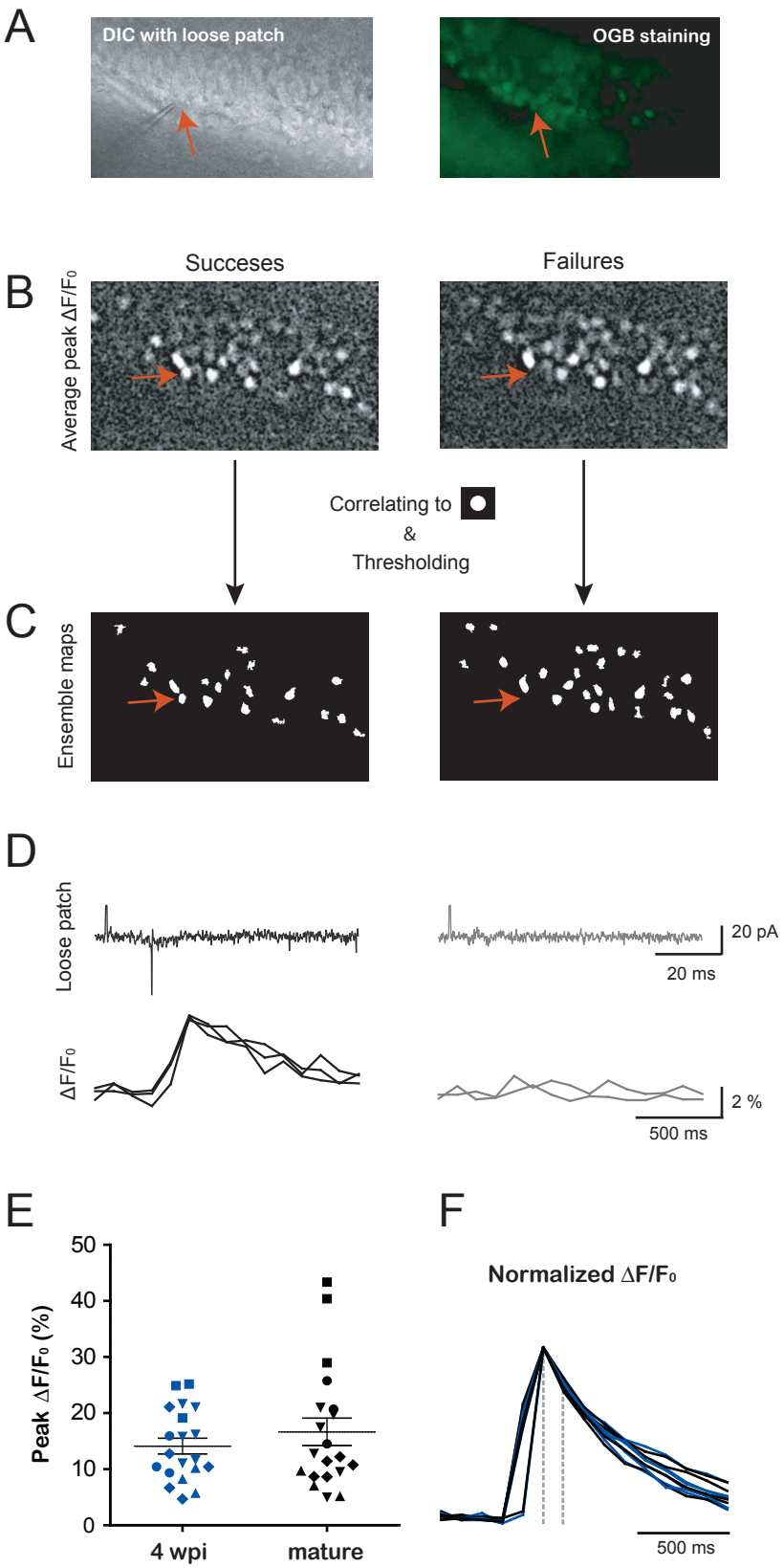
A
DIC with loose patch
OGB staining
B
Succeses
Failures
Average peak ΔF/F₀
Correlating to
&
Thresholding
C
Ensemble maps
D
Loose patch
20 pA
20 ms
ΔF/F₀
2 %
500 ms
E
Peak ΔF/F₀ (%)
50
40
30
20
10
0
4 wpi
mature
F
Normalized ΔF/F₀
500 ms

Fig. S2

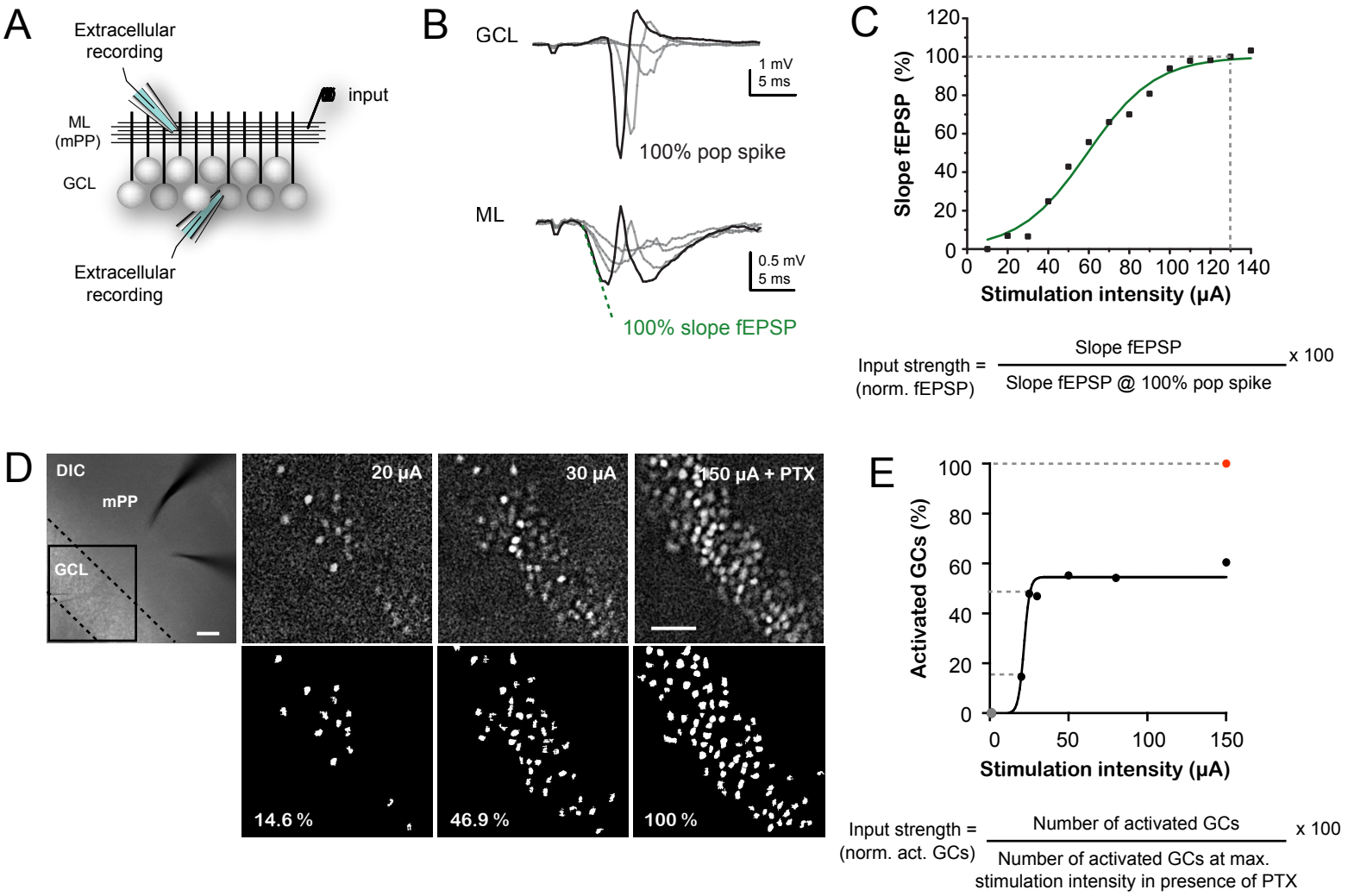
A
Extracellular recording
input
ML (mPP)
GCL
Extracellular recording
B
GCL
1 mV
5 ms
100% pop spike
ML
0.5 mV
5 ms
100% slope fEPSP
C
Slope fEPSP (%)
Stimulation intensity (µA)
Input strength (norm. fEPSP) = Slope fEPSP / Slope fEPSP @ 100% pop spike x 100
D
DIC
mPP
GCL
20 µA
30 µA
150 µA + PTX
14.6 %
46.9 %
100 %
E
Activated GCs (%)
Stimulation intensity (µA)
Input strength (norm. act. GCs) = Number of activated GCs / Number of activated GCs at max. stimulation intensity in presence of PTX x 100

Fig. S3

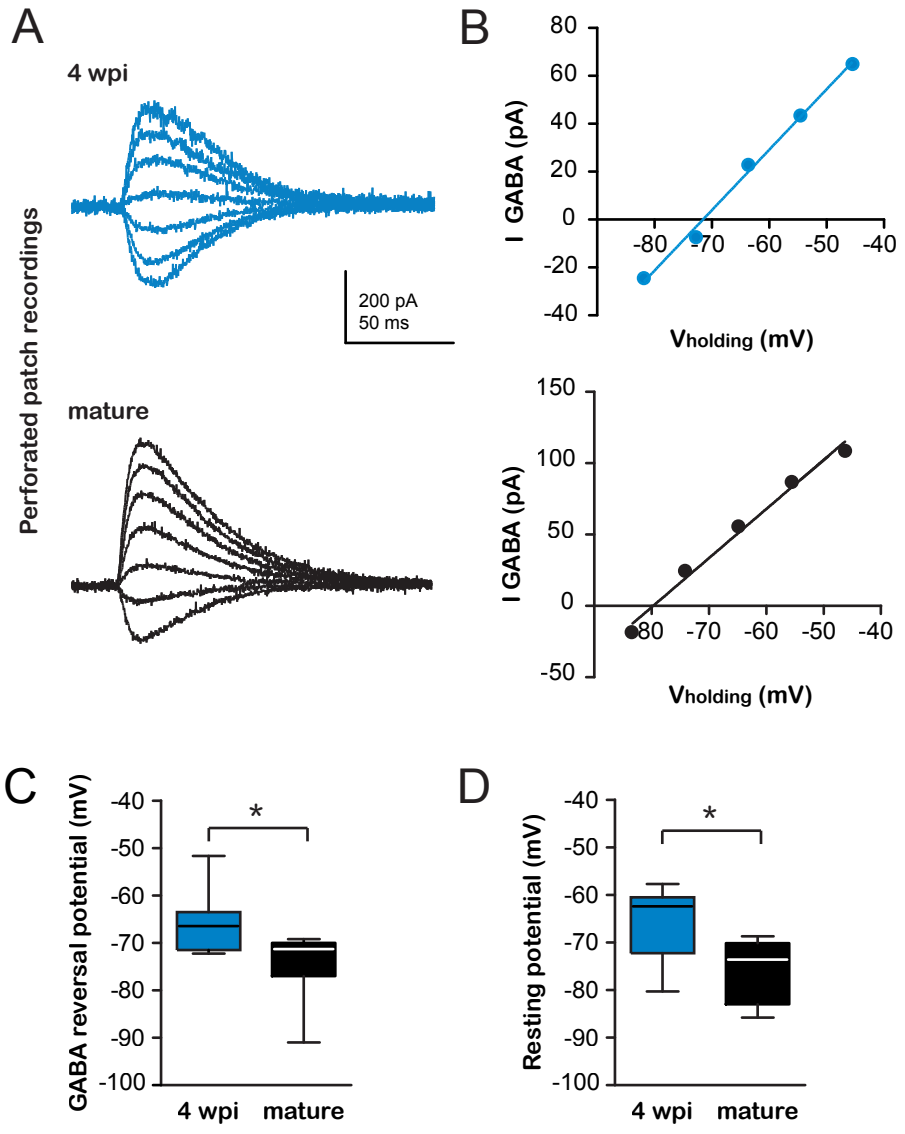
A
4 wpi
Perforated patch recordings
200 pA
50 ms
mature
B
I GABA (pA)
Vholding (mV)
C
GABA reversal potential (mV)
4 wpi
mature
D
Resting potential (mV)
4 wpi
mature

Fig. S4

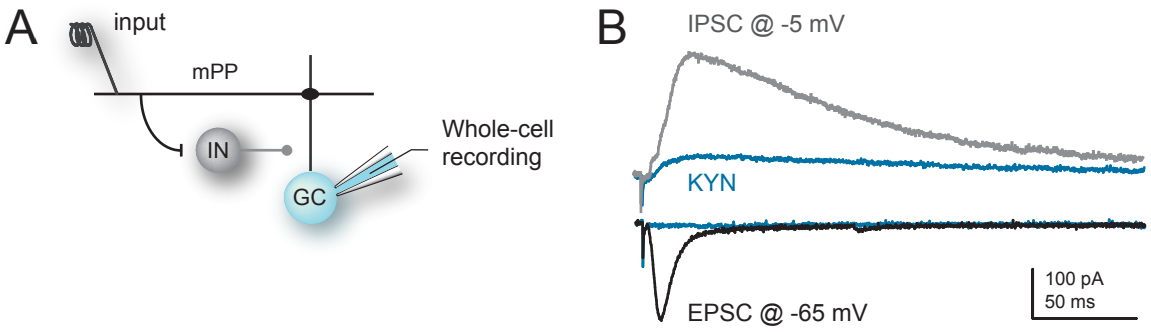
A
input
mPP
IN
GC
Whole-cell
recording
B
IPSC @ -5 mV
KYN
EPSC @ -65 mV
100 pA
50 ms

Fig. S5

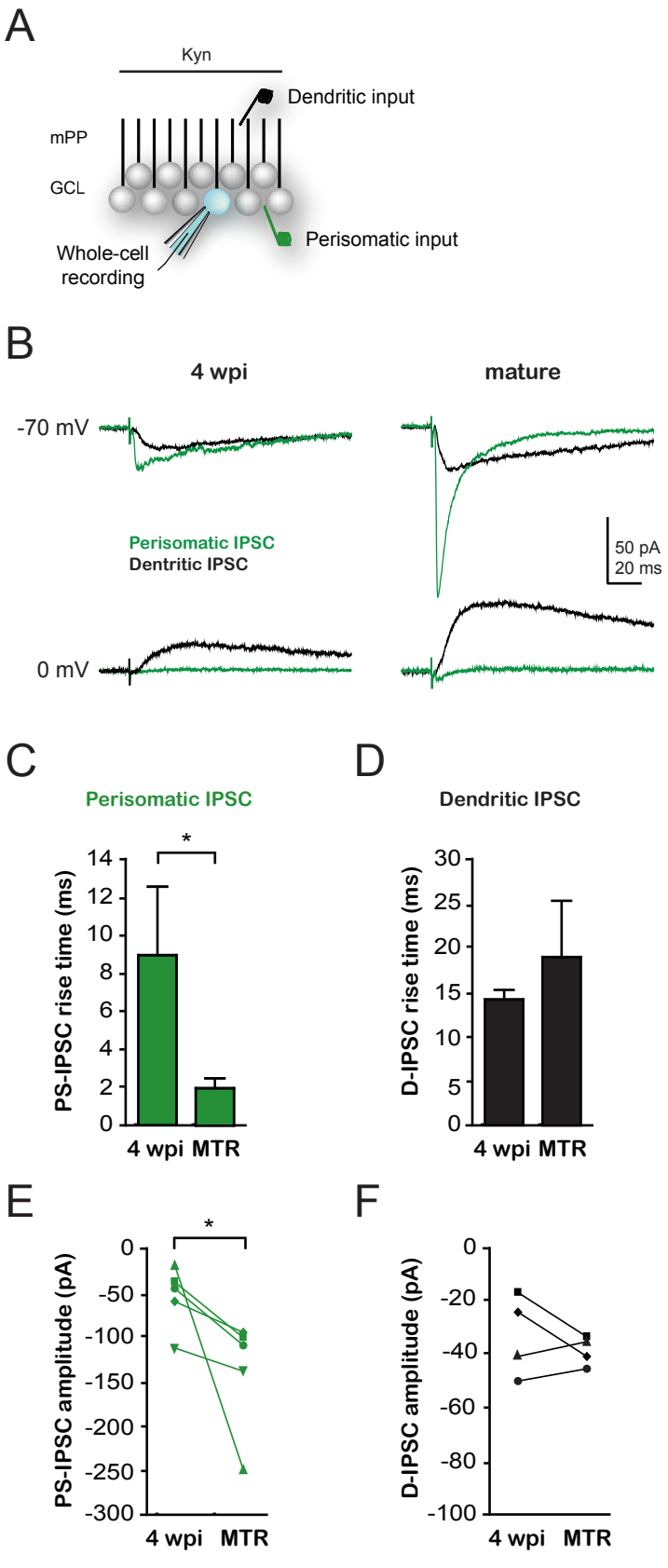
A
Kyn
Dendritic input
mPP
GCL
Perisomatic input
Whole-cell recording
B
4 wpi
mature
-70 mV
Perisomatic IPSC
Dentritic IPSC
50 pA
20 ms
0 mV
C
Perisomatic IPSC
PS-IPSC rise time (ms)
4 wpi MTR
D
Dendritic IPSC
D-IPSC rise time (ms)
4 wpi MTR
E
PS-IPSC amplitude (pA)
4 wpi MTR
F
D-IPSC amplitude (pA)
4 wpi MTR

Fig. S6

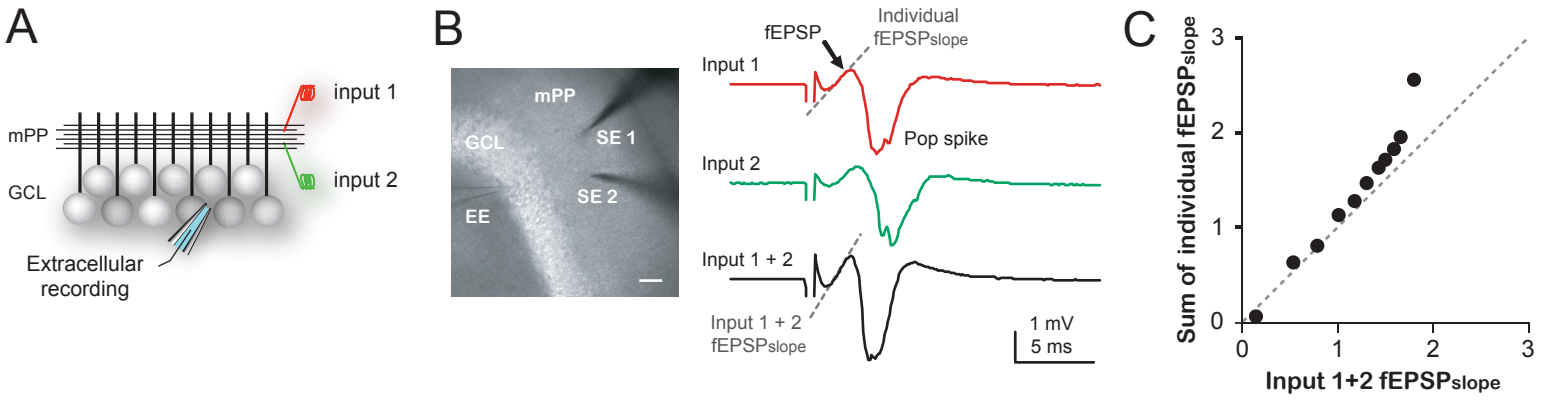
A
input 1
mPP
input 2
GCL
Extracellular
recording
B
mPP
GCL
SE 1
SE 2
EE
fEPSP
Individual
fEPSPslope
Input 1
Pop spike
Input 2
Input 1 + 2
Input 1 + 2
fEPSPslope
1 mV
5 ms
C
Sum of individual fEPSPslope
Input 1+2 fEPSPslope
0
1
2
3

Fig. S7

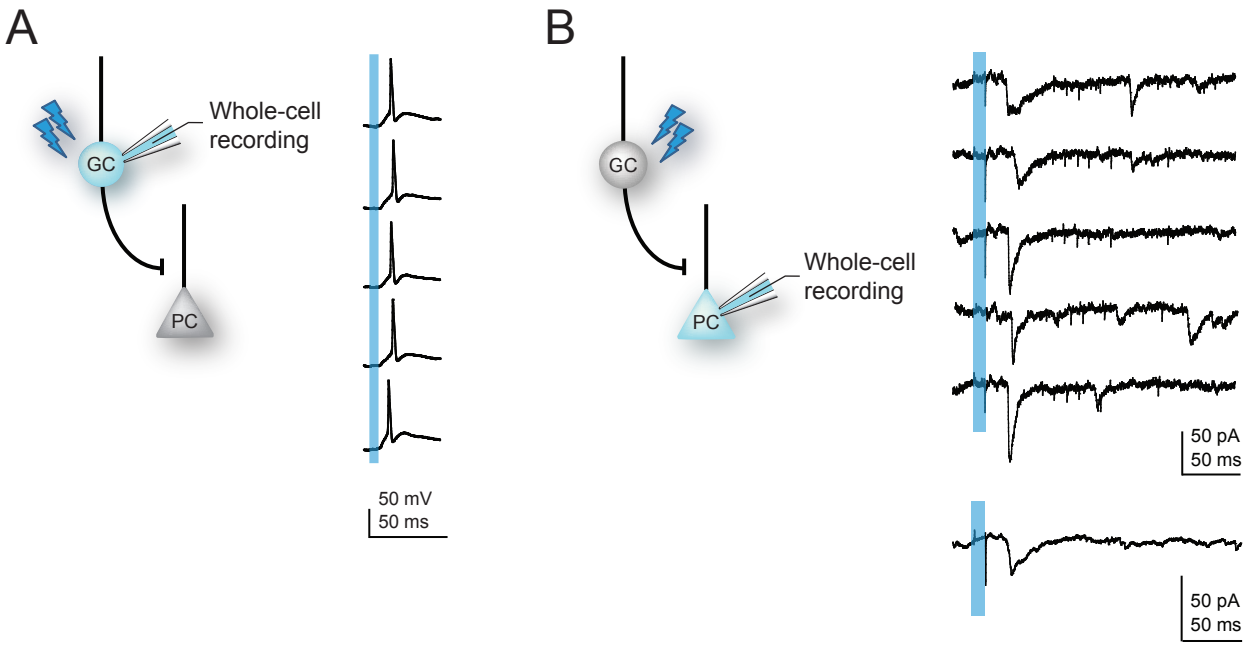
A
Whole-cell
recording
GC
PC
50 mV
50 ms
B
GC
PC
Whole-cell
recording
50 pA
50 ms
50 pA
50 ms

Fig. S8

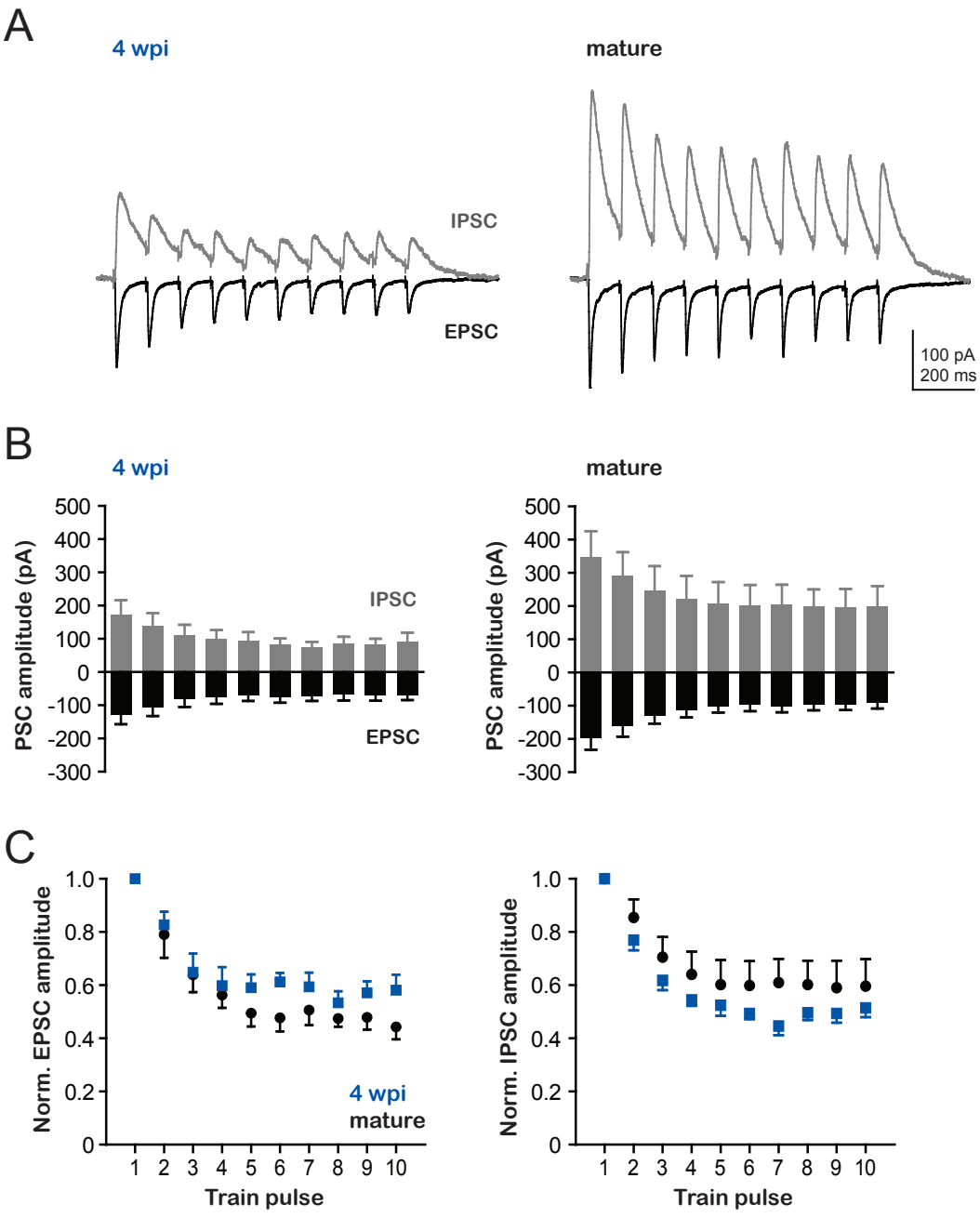
A
4 wpi
mature
IPSC
EPSC
100 pA
200 ms
B
4 wpi
mature
PSC amplitude (pA)
500
400
300
200
100
0
-100
-200
-300
IPSC
EPSC
C
Norm. EPSC amplitude
Norm. IPSC amplitude
1.0
0.8
0.6
0.4
0.2
0
1 2 3 4 5 6 7 8 9 10
Train pulse
4 wpi
mature

FIGURE LEGENDS

Fig. S1. Spiking detection in GC populations using calcium imaging in acute slices. (**A**) *Left,* DIC image of the GCL depicting a loose patch recording pipette onto a GC. *Right,* green fluorescence emission in the same area, loaded with the calcium indicator OGB-1 AM. Arrows indicate the position of the recorded cell. (**B**) Average of 5 trials of peak fluorescence ($\Delta F/F_o$) image in response to mPP stimulation. Note that images were sorted between spikes (left) or failures (right) of the recorded cell. (**C**) Ensemble binary maps of recruited GCs obtained by correlating average peak $\Delta F/F_o$ images with a circular template (diameter: 5.6 μm) and thresholding the correlation (see Methods). (**D**) Individual sweeps of loose patch recordings corresponding to the experiments shown above. Note the tight correspondence between success or failure observed in loose patch and imaging recordings. Panels **A-D** correspond to a single experiment. Similar results depicting the complete correspondence between calcium elevation and loose patch spikes were observed in 5 independent experiments. (**E-F**) Spiking evoked by mPP stimulation elicits calcium transients with similar amplitude and kinetics in 4 wpi and mature GCs. (**E**) Relative fluorescence intensity ($\Delta F/F_o$) for mPP-evoked spiking. Each dot represents the mean $\Delta F/F_o$ for 5 trials from a single GC. Different symbols denote data collected from different hippocampal slices. (**F**) Time-lapse measurements of normalized fluorescence intensity for 4 wpi (blue) and mature GCs (black). Each trace represent the mean time course for a given hippocampal slice (n = 3-6 neurons/slice). Dotted lines denote the time points utilized for spike detection.

Fig. S2. Input strength normalization. (**A-C**) Input normalization used for activation curves (**Fig. 1-3**). (**A**) Recording configuration: A stimulation electrode was placed to stimulate the mPP (input); one field recording electrode placed in the GCL and one in the molecular layer (ML) to simultaneously monitor the population spike (pop spike) and fEPSP, respectively. (**B**) Simultaneous recordings from the GCL (top) and ML (bottom) at increasing stimulus intensities. The input

strength is the slope of the fEPSP ($fEPSC_{slope}$, green line) elicited at any given stimulus intensity, normalized to the slope of the fEPSP evoked at the stimulus intensity that evokes a pop spike of maximal amplitude (100 %) (black traces; see methods for details and formula in panel C). (**C**) *Top*, normalized slope of the fEPSP (input strength) plotted against the applied current amplitude (stimulation intensity) for the experiment illustrated in B. Sigmoidal curves were fitted to the data; *bottom*, input strength calculation formula. (**D,E**) Input strength normalization used to measure input integration by calcium imaging (**Fig. 4**). (**D**) *Left*, example of an experiment showing the DIC image of a hippocampal slice with stimulating electrodes placed in the mPP and the extracellular electrode used to record the population activity (**see Fig. 4 and S6**). The calcium indicator OGB-1 AM was loaded in the GCL and the boxed area was used for time-lapse imaging. *Right*, top panels show a representative experiment displaying neuronal ensembles activated by one input at increasing current intensities (in μA), and the maximal neuronal activation obtained in the presence of PTX. *Bottom,* ensemble maps of the activated neurons corresponding to the top panels. The input strength was calculated as shown in E. (**E**) *Top*, normalized percentage of activated cells (input strength) plotted against applied current amplitude (stimulation intensity) for the experiment illustrated in D (sigmoidal fit to the data). Dashed lines denote values corresponding to the examples. *Bottom*, input strength calculation formula. The input strength is the number of activated cells at any given stimulus intensity normalized to the number of activated cells at the stimulus intensity that evokes maximal activation in the absence of GABAergic inhibition (100 %, value obtained in presence of PTX, red dot, see Methods). Scale bars: 50 μm.

Fig. S3. GABA reversal potential measured by gramicidin perforated patch. (**A**) Example experiments depicting perforated-patch voltage clamp recordings of currents elicited by focal application of GABA (20 μM) at different holding potentials from -80 mV to -40 mV in 4 wpi (blue)

and mature (black) GCs. (**B**) Peak I-V curves obtained from traces shown in A. (**C,D**) Differences in GABA reversal potential (C) and cell resting potential (D) between 4 wpi and mature GCs. (*, $p < 0.05$ *t*-test, n = 9 – 10 cells).

Fig. S4. Recording of monosynaptic EPSCs and di-synaptic IPSCs. (**A**) Scheme of a feed-forward inhibitory circuit and recording configuration showing the stimulating electrode (input) placed in the mPP, activated interneurons (IN) and activated GC recorded in whole-cell mode. (**B**) Whole cell current traces in response to mPP stimulation. Black: EPSC recorded in a GC held at -65 mV (the reversal potential of the IPSC). Gray: IPSC recorded at -5 mV (the reversal potential of the EPSC). Blue: Recordings in the presence of the glutamate receptor antagonist kynurenic acid (KYN) recorded at the corresponding potentials. Note that KYN abolishes both currents, indicating the disynaptic nature of the IPSC. Only recordings with >70% blockade by KYN (<30% of direct inhibition) were included in the analysis.

Fig. S5. Characterization of direct perisomatic and dendritic inhibition. (A) Schematic diagram of the recording configuration. Stimulating electrodes were placed in the granule cell layer (GCL) and the molecular layer to activate monosynaptic perisomatic or dendritic inhibition. Experiments were performed in the presence of 6 mM kynurenic acid (Kyn) to block glutamatergic transmission. IPSCs were subsequently measured in whole-cell recordings from individual cells. (B) Example traces of evoked perisomatic (green) and dendritic (black) IPSCs recoded at a membrane potential of -70 mV (*top*) or 0 mV (*bottom*) in 4 wpi and mature GCs. Note that perisomatic IPSCs display a reversal potential of ~0 mV due to the recording conditions under symmetrical Cl^-, while dendritic IPSCs display a positive driving force at that potential. (C, D) Analysis of rise time highlights a slower time course for perisomatic (PS-IPSC) but not dendritic (D-IPSC) responses in immature neurons (* denotes $p < 0.02$, *t-test;* n = 6 for S-IPSCs, n = 5 for D-IPSCs). (E, F) Paired

comparison of IPSC amplitudes indicates weaker perisomatic inhibition in immature GCs (* denotes $p < 0.05$, *t-test,* n = 5 for S-IPSCs and n = 4 for D-IPSCs). Data points were compared from neighboring 4 wpi and mature GCs recorded using the same stimulation intensity. Each data pair was obtained from a different slice.

Fig. S6. Range of stimulation to activate independent mPP inputs for imaging experiments. (**A**) Recording configuration: stimulation electrodes 1 and 2 were placed to stimulate independent mPP inputs. An extracellular recording electrode was placed in the GCL to monitor fEPSP and population spike. (**B**) *Left,* DIC image of a hippocampal slice with stimulating electrodes in the mPP and the extracellular recording electrode (EE) in the GCL. Scale bar: 50 µm. *Right,* fEPSP recordings in response to stimulation of inputs performed separately (1 or 2) or simultaneously (1+2). Dotted lines indicate the $fEPSP_{slope}$ for each response. (**C**) Sum of the individual $fEPSP_{slopes}$ plotted against the value obtained after simultaneous stimulation of inputs 1+2 for a typical experiment. All calcium imaging experiments were performed using stimulus strengths within the linear range.

Fig. S7. Immature (4 wpi) GCs release glutamate onto CA3 pyramidal neurons. (**A**) Left, schematic representation of the experimental procedure to record light-evoked spiking in 4 wpi GCs expressing channelrhodopsin-2 (ChR2). Right, example current-clamp traces of a 4 wpi GC spiking in response to blue light (blue line, 5 ms). (**B**) *Left*, schema illustrating the experimental procedure performed to detect light-evoked EPSCs on CA3 pyramidal neurons. *Right top*, example EPSCs recorded from a CA3 pyramidal neuron in response to 10-ms light pulses. Note that postsynaptic responses are time-locked to the light stimulus, while spontaneous activity is also observed. *Right bottom*, mean trace for 20 episodes denotes the prevalence of light-evoked EPSCs, whereas spontaneous activity is minimized after averaging. Similar responses were observed in 6 out of 9 recordings performed in CA3 pyramidal cells.

Fig. S8. Postsynaptic currents (PSCs) evoked by stimulus trains delivered to the mPP. (**A**) Examples of PSCs recorded in response to 10 Hz stimulation at 50 % of input strength obtained from 4 wpi and mature GCs. EPSCs (black traces) were recorded at a holding potential of -70 mV. IPSCs (gray) were recorded at 0 mV. (**B**) Peak PSC amplitudes for 4 wpi (left, n = 6) and mature GCs (right, n = 7). All PSC amplitudes display a depression for subsequent train pulses. (**C**) Normalized peak amplitude for EPSCs (left) and IPSCs (right) during train stimulation. Note that mature GCs display a marked depression in the amplitude of EPSCs, while immature GCs exhibit a marked reduction of IPSC amplitude. Differences in the extent of frequency depression were significant between 4 wpi and mature GCs after two-way ANOVA, with $p < 0.001$ (EPSCs) and $p < 0.001$ (IPSCs). Data represent mean ± SEM.

REFERENCES

1. D. A. Laplagne *et al.* Functional convergence of neurons generated in the developing and adult hippocampus. *PLoS.Biol.* **4**, e409 (2006).
2. Q. Yuan, J. S. Isaacson, M. Scanziani. Linking neuronal ensembles by associative synaptic plasticity. *PLoS One* **6**, e20486 (2011).
3. L. A. Mongiat, M. S. Espósito, G. Lombardi, A. F. Schinder. Reliable activation of immature neurons in the adult hippocampus. *PLoS.ONE.* **4**, e5320 (2009).
4. F. Pouille, A. Marin-Burgin, H. Adesnik, B. V. Atallah, M. Scanziani. Input normalization by global feedforward inhibition expands cortical dynamic range. *Nat Neurosci* **12**, 1577 (2009).
5. N. Toni *et al.* Neurons born in the adult dentate gyrus form functional synapses with target cells. *Nat.Neurosci.* **11**, 901 (2008).